SEICHING IN A LARGE WAVE FLUME

James T. Kirby[1], H. Tuba Özkan-Haller[2] and Merrick C. Haller[3]

Time series of cross-shore velocity and water surface elevation obtained during the
CROSSTEX laboratory experiment show the presence of low frequency motions that are
characteristic of the well-known phenomenon of wave basin seiching. In general, the modes
appear to be mostly standing in nature and the individual modes do not appear to be directly
forced by the paddle motions. A preliminary wavelet analysis shows they have well-defined
frequencies that are well-predicted by a linear analysis that treats the motions as unforced
standing waves. There are, however, some additional observed features that appear to be
unique to this case. For example, wavelet analysis also indicates a complex time dependence
of the modal amplitudes, which suggests the modes are interacting nonlinearly. In addition,
observations of the spatial mode structures hint at direct evidence of dissipation (such as wave
breaking) occurring in the higher modes. Finally, our initial nonlinear analysis approximately
reproduces the time scales for modal energy exchange observed in the experiments.

INTRODUCTION

The Cross-shore Transport Experiment (CROSSTEX) is a multi-investigator,
multi-university, scientific research project centered around a coordinated series
of near-prototype scale experiments that were conducted at Oregon State
University's O.H. Hinsdale Wave Research Laboratory (HWRL) during the
summer of 2005 (Maddux et al, 2006). The experiments took place in the 104m
long, 3.7m wide and 4.6m deep Large Wave Flume (LWF) on a movable bed
consisting of medium sand (d_{50}=0.22 mm). The objective of our portion of
the experiments was to obtain high-resolution observations related to onshore
and offshore sandbar migration. The analysis of seiching in the LWF was not
a primary objective of our experiments; however, our early analysis of the data
suggested they contained some unexpected behavior in regards to basin seiching.
Herein, we have pursued a detailed analysis of the observed low-frequency
motions as an "experiment of opportunity".

The experimental conditions consisted of irregular waves generated by
the paddle-type wavemaker with a range of peak periods (3-8 sec) and rms
wave heights (0.3m to 0.6m) depending on whether erosive or accretionary
conditions were desired. Observations of the hydrodynamics were carried out
using instruments mounted onto the walls of the flume, suspended from a
movable carriage, and remotely observed by video cameras as shown in Figure
1. The present analysis will utilize a limited number of Nortek Vectrino

[1] Center for Applied Coastal Research, University of Delaware Newark, DE 19716 USA
[2] College of Oceanic and Atmospheric Sciences, Oregon State University, Corvallis, OR 97331 USA
[3] Dept. of Civil, Constr.and Environmental Engineering, Oregon State University, Corvallis, OR 97331
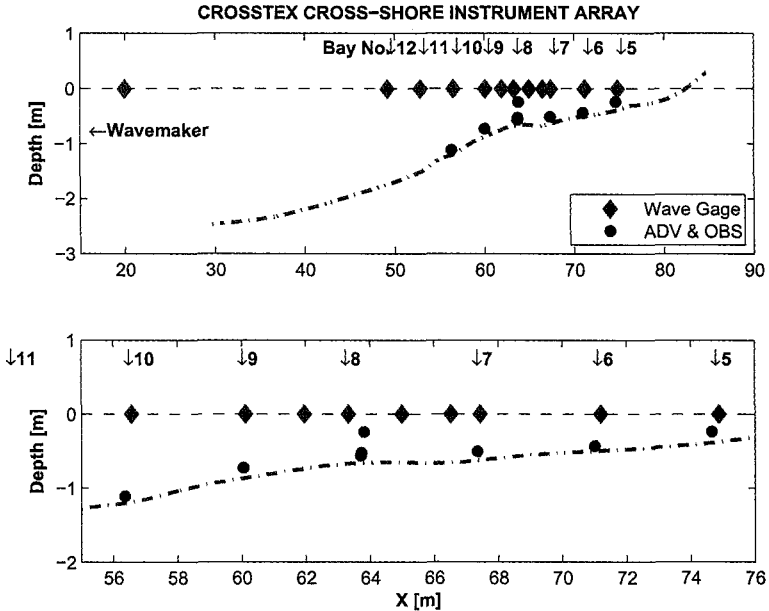USA

FIG. 1. Layout of tank and fixed instrumentation.

Doppler Velocimeters (NDV's), 12 wall-mounted surface piercing wave staffs, and measured bathymetry. The data encompassed more than 80 15-minute wave runs, of which several are used here. Standard procedure was to collect data for 20 minutes with active wave generation occurring in the center of this window. The results shown here are representative of the the accretional portions of the experiment (peak period of 8 seconds).

In the following, we first examine the behavior of low frequency motions in the LWF and compare the dominant observed spectral peaks with the principal standing wave modes in the tank as predicted by linear theory. We then develop the free wave evolution equations appropriate to weakly nonlinear standing motions in this system, and show that predicted time scales for modal energy exchange are consistent with the observations. Finally, we provide evidence that dissipation is occurring in the higher standing modes, which may take the form of intermittent breaking.

OBSERVATIONS OF SEICHING

A typical time series from a 20 minute data run is shown in Figure 2. The time axis represents the time from the onset of data acquisition (not the onset of paddle motion) and the time series shows the presence of low frequency motion, which
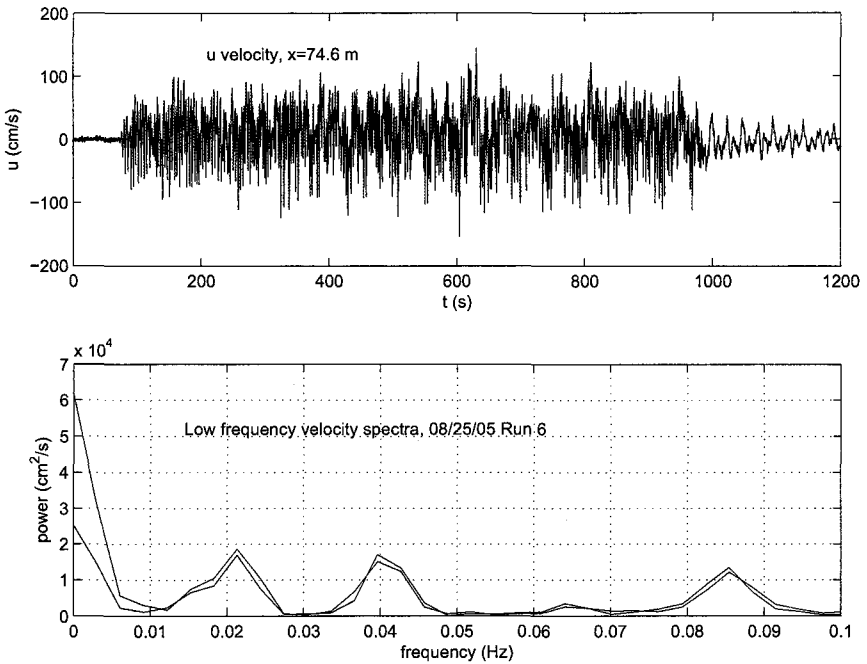
FIG. 2. **Time series and power spectral density for NDV velocity record at** $x = 74.6m$, **08/25/05 Run 6.**

is most clearly seen after the wave paddle has stopped and the last incident wave has passed the instrument ($t > 1000$ sec for this record). A Fourier transform of these data shows the presence of isolated peaks at low frequencies (lower panel, Figure 2). In this particular plot, there is only a weak spectral peak at 0.065 Hz due to the location of the current meter near a cross-shore node for this particular mode and this particular run.

In order to determine how quickly these motions were established in the tank, we performed a preliminary analysis of the data using the continuous wavelet transform (Farge, 1992). A Morlet wavelet was used and results are shown in Figure 3 as the modulus of the transform for frequencies below 0.1 Hz. The growth of energy in frequency bands corresponding to the spectral peaks in Figure 2 is apparent, with the peak near 0.085 Hz gaining energy first. It is also apparent that the individual spectral peaks experience unsteadiness in amplitude. It is possible that this is due to direct forcing by the wave groups associated with the train of random incident waves. However, there appears to be a pattern to the gain and loss of energy in the individual modes. For example, the mode near 0.04 Hz appears to peak in amplitude around $t = 700s$, near a minimum of the higher frequency peak and before the peak in the lower frequency around 0.02 Hz occurs.
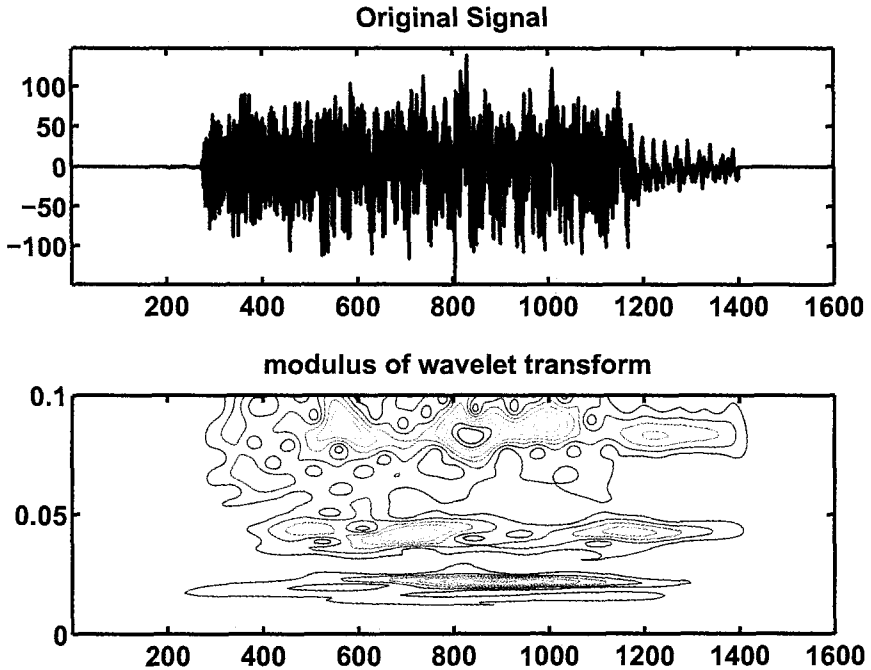
Original Signal

modulus of wavelet transform

FIG. 3. Wavelet analysis of low frequency motion in tank, same conditions as Figure 2. Upper panel: time series of on-offshore velocity. Lower panel: Modulus of Morlet wavelet transform for the frequency range $0 \leq f \leq 0.1Hz$. Note structure of results near $f = 0.02Hz, 0.04Hz, 0.06Hz$ and $0.08Hz$, which are identified with seiching modes 1, 2, 3 and 4 below.

In contrast, at $t = 900 - 1000s$, the peak near 0.04 Hz is nearly gone while the peaks at 0.02 and 0.08 Hz take on their largest values. The behavior shown here is suggestive of a significant energy exchange between individual spectral peaks due to nonlinear interaction, as examined below.

LINEAR EIGENMODE ANALYSIS

We consider small amplitude seiching in a 1-D horizontal canal of depth $h(x)$ and spanning the interval $0 \leq x \leq L$, bounded at $x = 0$ by a vertical wall and at $x = L$ by a sloping beach. The governing equations are given by the linear long wave equations

$$\eta_t + (hu)_x = 0 \tag{1}$$

$$u_t + g\eta_x = 0 \tag{2}$$

where u is horizontal velocity and η is water surface displacement. At $x = 0$,

impermeability of the wall and inspection of (2) gives

$$u = \eta_x = 0; \qquad x = 0 \tag{3}$$

At the sloping boundary $x = L$, we require that the motion remain bounded. We may eliminate either u or η between (1) and (2) to obtain either

$$\eta_{tt} - g(h\eta_x)_x = 0; 0 \le x \le L \tag{4}$$

or

$$u_{tt} - g(hu)_{xx} = 0; 0 \le x \le L \tag{5}$$

together with the described boundary conditions on u or η.

For the case of time-harmonic motion with angular frequency ω, equations (4) and (5) may be rewritten as

$$(h\eta_x)_x + \lambda\eta \;\; = \;\; 0 \tag{6}$$
$$(hu)_{xx} + \lambda u \;\; = \;\; 0 \tag{7}$$

where $\lambda = \omega^2/g$ represents the eigenvalue for the problem. We note that (6) together with the sloping shoreline boundary condition does not represent a standard Sturm-Liouville problem due to the boundary condition at the shoreline. Nevertheless, it is simple to show that an expansion in the form

$$\eta = \sum_{n=1}^{\infty} \eta_n G_n(x) \tag{8}$$

leads to the orthogonality condition

$$\int_0^L G_n G_m dx = 0; n \ne m \tag{9}$$

and, for $n = m$, a statement of the dispersion relation for each mode given by

$$\omega_n^2 = -g\frac{\int_0^L h(G_n')^2 dx}{\int_0^L G_n^2 dx} \tag{10}$$

Equation (5) also is not in Sturm-Liouville form. The Liouville transformation leads to the choice of volume flux $q = hu$ as the dependent variable, giving the equation

$$q_{xx} - \lambda h^{-1} q = 0 \tag{11}$$

together with homogeneous boundary conditions $q(0, L) = 0$, where the homogeneous boundary condition at a sloping shoreline arises by virtue of the
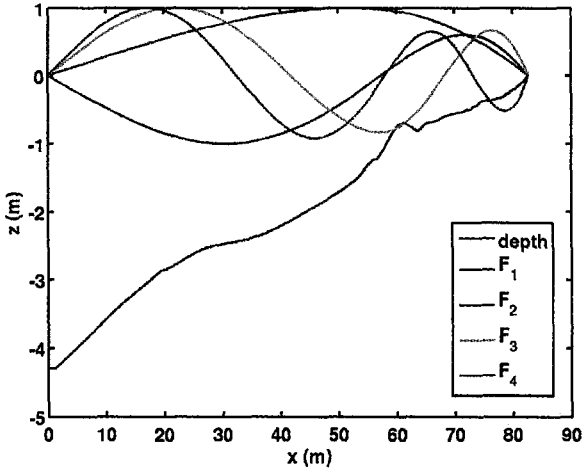
FIG. 4. Eigenmodes $F_1 - F_4$ for volume flux q for profile measured on 8/22/05.

zero in water depth. The corresponding expansion, orthogonality condition, and dispersion relation are given by

$$q(x) = \sum_{n=1}^{\infty} q_n F_n(x) \tag{12}$$

$$\int_0^L h^{-1} F_n F_m dx = 0; \qquad n \neq m \tag{13}$$

$$\omega_n^2 = -g \frac{\int_0^L (F_n')^2 dx}{\int_0^L h^{-1} F_n^2 dx} \tag{14}$$

In this study, we have chosen to solve (11) numerically in order to determine the family of eigenmodes for measured tank geometry. The equation is finite differenced using centered second-order derivatives, and the resulting matrix eigenvalue problem is solved using the Matlab routine EIG.

Modal amplitudes: an example from the tank

An example set of the the 4 lowest modes $F_1 - F_4$ in the tank are shown in Figure 4 for a profile measured on 8/22/05. Corresponding modes for surface displacement $G_n = dF_n/dx$ are shown in Figure 5.

Mode periods are computed from the eigenvalues of the numerical solution based on measured bathymetry for each run. A comparison of numerically predicted mode periods to measured mode periods is shown in Figure 6.
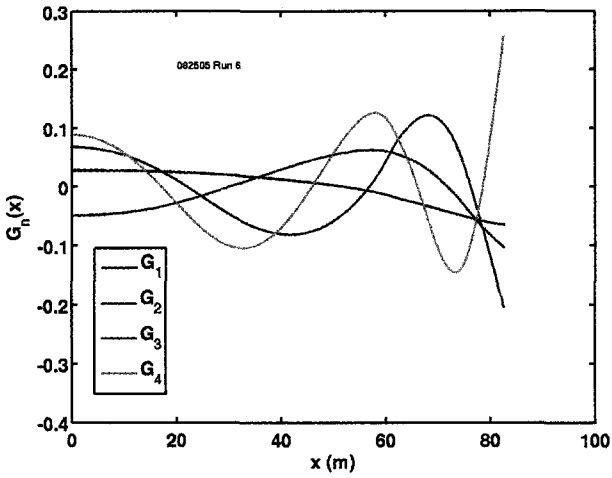
FIG. 5. Eigenmodes $G_1 - G_4$ for surface displacement η for profile measured on 8/22/05.
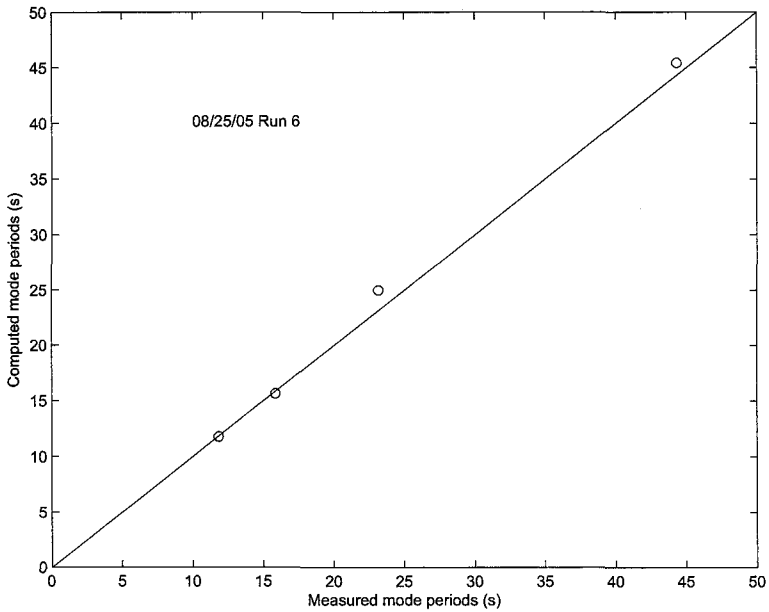

FIG. 6. A comparison of numerically predicted mode periods to measured values: 08/25/05 Run 6.

A time series for each of the individual modes is computed as follows. First, the wave gage data for the 12 gages mounted along the tank wall (Figure 1) are band-passed for each predicted mode frequency, $0.8f_n < f < 1.2f_n, n = 1, 2, 3, 4$. Then, for each mode n, the numerically predicted $G_n(x_i)$ is projected onto the bandpassed data $\eta(x_i, t)$ to give a single times series $A_n(t)$. Here, x_i are gage locations in the flume. Figure 7 displays the time history $A_n(t)$ for the first 4 modal amplitudes. Then, the motion of each mode at each gage is reconstructed according to $\eta_n(x_i, t) = G_n(x_i)A_n(t)$.

The results in Figure 7 show a pattern of energy exchange between modes, with modulations occuring more rapidly at higher mode numbers. The growth and decay of the fundamental mode 1 occurs over a time scale on the order of 500-600s, slightly shorter than the entire data run duration. The drop in amplitude of the mode 1 peak starts at around 700s, clearly before the cessation of forcing around $t = 960s$. Modal evolution times for the higher modes are much shorter, on the order of 200-300 seconds for mode 2 and 100-200 seconds for modes 3 and 4. Note also that mode 3, which was largely missing in the single current meter record examined above, is energetic and shows up clearly in the surface displacement time series.

NONLINEAR THEORY

Based on the previous examination of the time history of modal amplitudes for the observed low-frequency motions, we hypothesize that nonlinear interactions are contributing significantly to the evolution of these amplitudes, by way of allowing for energy transfer between the standing wave modes. In order to examine this hypothesis, we use a perturbation expansion based on the assumption of weak nonlinearity, applied to the nonlinear shallow water equations (NLSE). The resulting theory is in the form of coupled evolution equations for the modal amplitudes. The resulting interaction equations are detuned in the sense that significant mismatch exists in the sums of interacting frequency triads, but we observe that the resulting interactions occur on timescales which are in reasonable agreement with observations.

Formulation

In order to proceed, we nondimensionalize x by L, h by maximum depth h_0, η by an amplitude scale a and time t by L/c_0 where $c_0 = \sqrt{gh_0}$ is the long wave speed in the deepest portion of the basin. Letting $\delta = a/h_0$, we obtain the scaled equations

$$\eta_t + \delta q_x + (h^{-1}\eta q)_x = 0 \tag{15}$$

$$q_t + \delta q(h^{-1}q)_x + h\eta_x = 0 \tag{16}$$

or, eliminating η in $O(1)$ terms,

$$q_{tt} - hq_{xx} + \delta \left\{ \left[q(h^{-1}q)_x\right]_t - h[h^{-1}\eta q]_{xx} \right\} = 0 \tag{17}$$
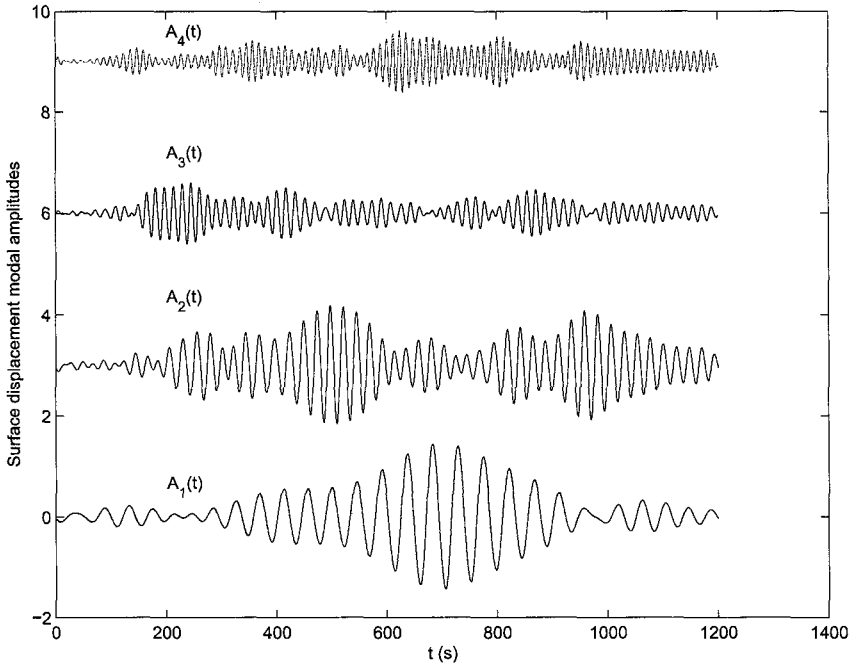
FIG. 7. Modal amplitudes $A_1(t) - A_4(t)$ for the 08/25/05 Run 6 data. Short wave forcing begins at $t = 60s$ and ends at $t = 960s$. The initial concentration of seiching energy in higher modes, and the subsequent transfer to, and then from, mode 1 is evident.

As in the previous section, the boundary condition at a wall boundary is taken to be $q = 0$. At a sloping boundary, however, we must account for the motion of the shoreline, which we take to have instantaneous horizontal position $\delta\xi(t)$ relative to the still water shoreline. At this point, the discharge based on total depth $H = h + \delta\eta$, given by $Q = uH$, drops to zero. We introduce perturbation expansions

$$q = q_0 + \delta q_1 + ... \qquad (18)$$

$$\eta = \eta_0 + \delta\eta_1 + ... \qquad (19)$$

and further introduce a multiple scale expansion for fast and slow time scales

$$t \rightarrow t + \delta t + ... = t + T_1 + ... \qquad (20)$$

The leading order solution follows from the previous section and may be written as

$$q_0(x, t) = \sum_{n=1}^{\infty} q^n(t, T_1) F_n(x) \qquad (21)$$

where the F_n's are solutions to (11). We write the q^n in terms of slowly varying amplitudes as

$$q^n(t, T_1) = \frac{1}{2}(a_n(T_1)E_n + a_n^*(T_1)E_{-n}); \qquad E_n = e^{i\omega_n t} \qquad (22)$$

Equations for Detuned Triad Interactions

Use of (22) in the governing equation for q_1 leads to a coupled set of evolution equations for modal amplitudes $a_n(T_1)$, with the interactions resulting from energy exchange through detuned triads. The evolution equations are given schematically by

$$\frac{\partial a_n}{\partial T_1} = \frac{1}{8\omega_n I_n} \left\{ \sum_l R_{n,l,n-l} a_l a_{n-l} E_{n-l,l,-n} + \sum_l S_{n,l,l-n} a_l a_{l-n}^* E_{l,n-l,-n} \right.$$

$$\left. + \sum_l T_{n,l,n+l} a_l^* a_{n+l} E_{n+l,-l,-n} \right\} \qquad (23)$$

with

$$E_{\pm a, \pm b, \pm c} = e^{i(\pm\omega_a \pm \omega_b \pm \omega_c)t} \qquad (24)$$

Here, the factors E express the detuning of the underlying triads resulting from non-commensurate linear mode frequencies. This detuning would drop to zero in a rectangular, flat-bottomed tank, but is on the order of 10% for the nearly triangular geometry studied here.

The system described here does not incorporate either the forcing due to incident short waves or dissipation, and thus represents a conservative system. Solutions involving more than 3 modes are essentially chaotic. Since we do not have a means of predicting modal amplitudes in the absence of forcing and dissipation, we choose a set of initial amplitudes of reasonable size compared to the data. Figure 8 shows a representative calculation. We note that the time scales for evolution of the various modes vary from 600-700 seconds for the fundamental mode 1, down to around 200 seconds for the highest mode 4. These periods are slightly long compared to observed data, but the overall conclusion is that, in the absence of any fine tuning corresponding to the introduction of forcing and damping, the theory appears to provide a reasonable estimate for the overall time scale for energy exchange in the flume.

INTERMITTANT BREAKING OF SEICHE MODES

The analysis above depends heavily on the assumption that low frequency motion in the tank is described by a superposition of standing waves. A quick analysis of a water surface constructed by examining the band-passed time series for each gage location, $\eta(x_i, t)$ confirms this assumption for the most part for the lower two mode numbers. However, an examination of the higher mode number motions suggests that progressive modes are also present.
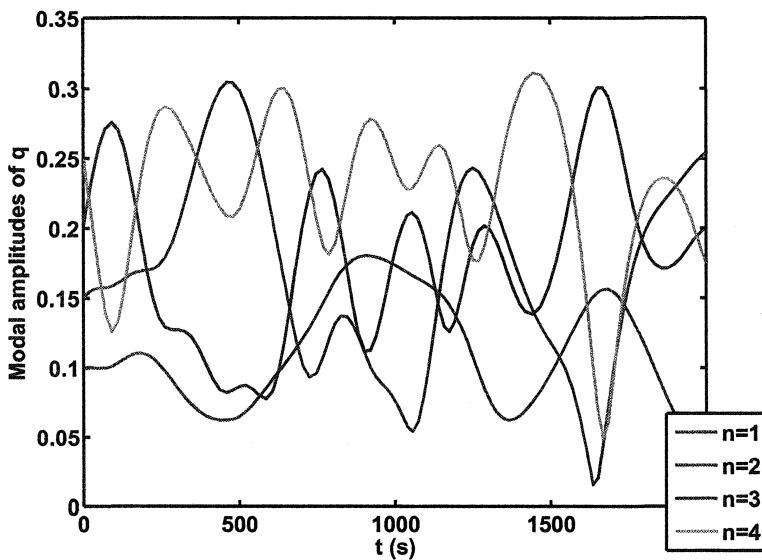
FIG. 8. Nonlinear energy exchange between modes 1-4 for the measured bathymetry of 08/25 Run 6. Arbitrary initial conditions.
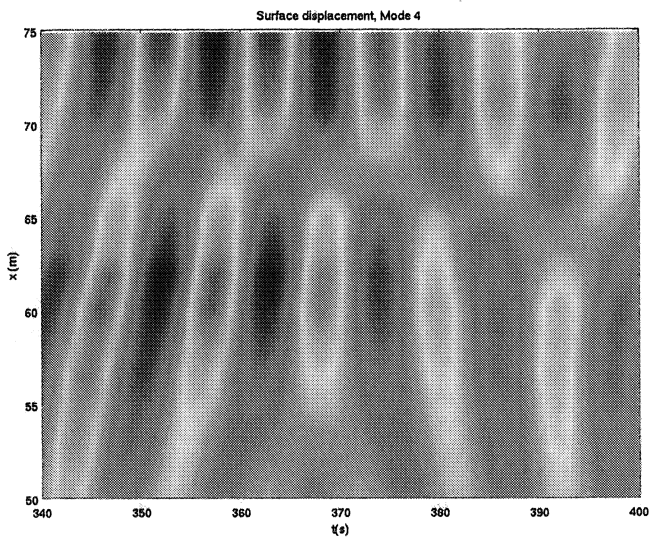

FIG. 9. Measured surface displacement $\eta(x_i, t)$ for a band pass around $n = 4$, for a window $340s < t < 400s$. Standing wave behavior.
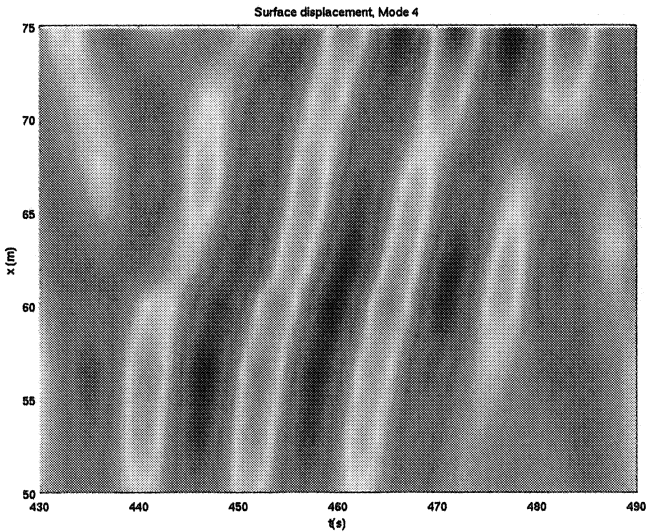
Surface displacement, Mode 4

FIG. 10. **Measured surface displacement** $\eta(x_i, t)$ **for a band pass around** $n = 4$, **for a window** $430s < t < 490s$. **Progressive wave behavior.**

Figures 9 and 10 show plots of surface elevation time series from all the wall-mounted wave gages. The time series have been bandpassed about the mode 4 frequency and each plot shows a different 60 second window. Figure 9 shows a pattern that is mainly consistent with a standing wave pattern with a node around $x = 65m$ (see the corresponding pattern for G_4 in Figure 5.) The nodal position shifts slowly in the offshore direction but is present for the entire window. In contrast, Figure 10 illustrates a transition to progressive wave behavior in the middle of the window, with standing wave behavior near the beginning and end of the window. The trajectory of the crest position in the middle of the window is consistent with a phase speed of $\sqrt{gh}$. The centers of these two windows are 90 seconds apart, indicating that there is a rapid transition between standing and progressive wave behaviors. This result indicates that dissipation plays a potentially important role in the evolution of at least some of the seiching modes, and that the description of the low-frequency motion may need to be done in terms of superposed progressive solutions instead of simple standing waves.

We note that Van Dongeren et al (2006) have described laboratory experiments involving low-frequency waves forced at the difference frequency of incident bichromatic wave trains, in which the behavior of the low-frequency wave was clearly consistent with the occurrence of breaking of the forced wave. The resulting forced motion was regular and periodic. However, we do not know of

previously reported observations in which a particular seiching mode shifts from standing to breaking/progressive on a time scale which is of the order of only a few periods of the mode in question. This behavior greatly complicates the overall problem of describing the low frequency motion, and needs further examination.

CONCLUSIONS

Analysis of data from a large scale laboratory experiment demonstrates the presence of multiple low-frequency motions, which are generally similar to classical linear standing waves (seiching). However, there are some unexpected aspects to the present observations. First, though spectral analysis indicates the modes have well-defined frequencies, a wavelet analysis suggests that individual modes are exchanging energy through nonlinear interactions. A calculation of the linear seiching modes well-predicts the observed frequencies. A preliminary nonlinear calculation, that treats the seiching modes as weakly nonlinear, unforced standing waves, also does well at reproducing the time scales of modal energy exchange. Finally, observations also suggest that dissipation, such as wave breaking, of the higher seiching modes may play a significant role in the modal amplitude evolution.

REFERENCES

Farge, M., 1992, "Wavelet transforms and their applications to turbulence", *Ann. Rev. Fluid Mech.*, **24**, 395-457.

Maddux, T. B., Cowen, E. A., Foster, D. L., Haller, M. C. and Stanton, T. P., 2006, "The cross-shore sediment transport experiment (CROSSTEX)", *Proc. 30th Intl. Conf. Coastal Engrng*, San Diego, in press.

van Dongeren, A., Battjes, J., Janssen, T., van Noorloos, J., Steenhauer, K., Steenbergen, G. and Reniers, A., 2006, "Shoaling and shoreline dissipation of low-frequency waves", *J. Geophys. Res.*, in press.